

# Aqueous solvation dynamics studied by photon echo spectroscopy

M. J. Lang,<sup>a)</sup> X. J. Jordanides,<sup>b)</sup> X. Song,<sup>c)</sup> and G. R. Fleming<sup>b,d)</sup>

*Department of Chemistry and the James Franck Institute, The University of Chicago, Chicago, Illinois 60637 and Department of Chemistry, University of California, Berkeley and Physical Biosciences Division, Lawrence Berkeley National Laboratory, Berkeley, California 94720*

(Received 17 July 1998; accepted 17 December 1998)

Three-pulse photon echo peak shift measurements were employed to study aqueous solvation dynamics. A new perspective of dielectric continuum theory [X. Song and D. Chandler, *J. Chem. Phys.* **108**, 2594 (1998)] aided in characterizing the system-bath interactions of eosin in water. Application of this theory provides solvation energies, which were used within the spectral density representation  $\rho(\omega)$ , to calculate the experimental peak shift. Simulations with only solvation contributions to  $\rho(\omega)$ , where a substantial amplitude of the solvation occurs within  $\sim 30$  fs, are remarkably consistent with our data. Furthermore, simulations using this theoretical solvation spectral density and an experimentally determined intramolecular spectral density yield an excellent total simulation of the peak shift data over the entire dynamic range. Our experimental results substantiate predictions that interaction-induced polarizability effects, contributing via a  $\sim 180$   $\text{cm}^{-1}$  band in the spectral density, influence the initial dynamics. © 1999 American Institute of Physics. [S0021-9606(99)50312-7]

## I. INTRODUCTION

Determination of the structural and dynamical properties of liquid water is a major area of investigation both experimentally<sup>1-15</sup> and theoretically.<sup>16-20</sup> Experimentally, time-domain techniques such as fluorescence up-conversion,<sup>2</sup> optical Kerr effect (OKE)<sup>3-5</sup> and THz spectroscopy,<sup>6,7</sup> in addition to frequency-domain spectroscopies such as Raman<sup>8-10</sup> and infrared (IR)<sup>11-15</sup> have been employed to gain a detailed understanding of the intermolecular and intramolecular motions and dynamics of liquid water. Theoretical studies of aqueous solvation<sup>16</sup> have included simulations ranging from predictions of the IR and Raman spectra,<sup>20-23</sup> to calculations of the solvation relaxation function  $S(t)$ ,<sup>17,19,23,24</sup> and the third order response.<sup>26,27</sup> In addition, normal-mode investigations have aided in understanding the short-time dynamics of water.<sup>28,30</sup>

It has been previously shown experimentally that aqueous solvation dynamics contains much shorter time scales than other solvent systems. However, the ability to experimentally resolve the shortest solvation time scale has been limited by the instrument response. Barbara *et al.*<sup>1</sup> reported two exponential solvation components,  $\sim 250$  fs, and 1.2 ps, and Jimenez *et al.*,<sup>2</sup> via a time dependent fluorescence Stokes shift measurement of C343 in water, showed that water solvation was even faster. The resulting solvation time correlation function contained an initial decay of 55 fs (with 50% of the amplitude) which was attributed to librational solvent motions.<sup>2</sup> This 55 fs solvation component represents the fastest observable solvation time scale, as a result of the dynam-

ics being convoluted by the instrument response. Recently, Huppert and co-workers<sup>3</sup> also resolved a bimodal behavior, in a study of rhodamine 800 in water, with an ultrafast component of less than 100 fs.

Theoretically, water solvation is predicted to be even faster. Maroncelli and Fleming,<sup>17</sup> using molecular dynamics simulations, and later, Bader and Chandler<sup>18</sup> predicted an even larger amplitude decay,  $\sim 70\%$ – $90\%$ , with faster (25 fs) dynamics. Song and Chandler,<sup>19</sup> using the full range of dynamic dielectric continuum theory, reconstructed a theoretical solvation time correlation function,  $S(t)$ , for direct comparison with the fluorescence upconversion experiment of Jimenez *et al.*<sup>2</sup> The theoretically predicted dynamics is again much faster than those observed in past experiments.

The present study provides experimental confirmation of these theoretical predictions. The ultrafast dynamics of the aqueous system results from large amplitude, high-frequency intermolecular librational and vibrational motions.<sup>2</sup> Water exhibits motions ranging from sub-wavenumber to 3500  $\text{cm}^{-1}$ , revealed by the spectral density of Fig. 1. These motions correspond to time scales from picoseconds to a few femtoseconds. Because many of the characteristic intermolecular frequencies of liquid water are well above room temperature energies,  $k_B T = 207$   $\text{cm}^{-1}$ , the ongoing discussion of whether a complete description of aqueous dynamics requires a quantum mechanical treatment persists.<sup>23,29</sup>

An extensive theoretical pursuit of the origin of the low-frequency ( $3$ – $250$   $\text{cm}^{-1}$ ) intermolecular components of hydrogen bonded network of liquid water, has persisted for over a decade.<sup>20-27</sup> Madden and co-workers<sup>20</sup> established that the appearance of the hindered translational features (near 60 and 200  $\text{cm}^{-1}$ ) observed in the IR and Raman spectra of water are due to interaction-induced dipoles. This first report initiated theoretical investigations<sup>21-27</sup> to determine the role, if any, of the electronic polarizability on these low-

<sup>a)</sup>Department of Molecular Biology and Princeton Materials Institute, Princeton University, Princeton, New Jersey 08544.

<sup>b)</sup>University of California and Berkeley National Laboratory.

<sup>c)</sup>Department of Chemistry, Iowa State University, Ames, IA 50011.

<sup>d)</sup>Corresponding author; e-mail address: GRFleming@lbl.gov

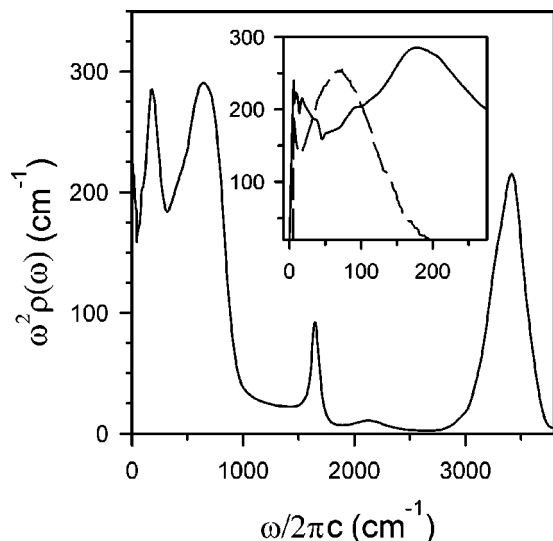


FIG. 1. The coupling strength weighted spectral density  $\rho(\omega)\omega^2$  of the theoretical solvation contribution for water (solid line) constructed by the method of Ref. 19. The spectral density for acetonitrile is shown in the inset (dashed line) along with the low-frequency region of the water spectral density. The acetonitrile spectral density (Ref. 31) shows a band centered at  $\sim 80 \text{ cm}^{-1}$  attributed to the librational motion that dominates polar solvation.

frequency motions of liquid water. Recently, a calculated third order response function, including an interaction-induced term,<sup>26,27</sup> concurred with experimental OKE data of pure water.<sup>4,5</sup> However, a solvation dynamics study has not yet experimentally resolved the influence of this dipole-induced-dipole contribution in water.

A theoretical solvation spectral density of water is compared to acetonitrile<sup>31</sup> in the inset of Fig. 1. The acetonitrile spectral density exhibits a broad band peaking at  $\sim 80 \text{ cm}^{-1}$  attributed to librational solvent motion. The peak at  $\sim 2.5 \text{ cm}^{-1}$  corresponds to a 2 ps diffusive solvation component. It is commonly accepted that the librational contribution dominates solvation in acetonitrile and other polar solvents (e.g., methanol).<sup>31-34</sup> The solvation contribution is easily extracted from experiments with adequate time resolution because it acts on a different time scale than intramolecular contributions to the optical response. By contrast, the solvation spectral density of water reveals a much more complex picture. The intermolecular components between 0 and  $1000 \text{ cm}^{-1}$  in the solvation spectral density have been assigned to diffusive motions ( $\sim 2-10 \text{ cm}^{-1}$ ), a hindered translational region of the hydrogen-bonded network ( $\sim 180 \text{ cm}^{-1}$ ), and a broad hindered rotational (librational) band ( $\sim 600 \text{ cm}^{-1}$ ).<sup>16</sup> The band observed at  $60 \text{ cm}^{-1}$  in the Raman<sup>8-10</sup> and OKE<sup>3-5</sup> spectra is assigned to the hydrogen bonding bend. However, its appearance in the far IR is more controversial.<sup>6,15,22</sup> The experimental data<sup>13,14</sup> used to calculate the spectral density in this range resolves a broad and very weak shoulder on the  $200 \text{ cm}^{-1}$  band at  $50 \text{ cm}^{-1}$ , which presumably corresponds to the shoulder at  $\sim 40 \text{ cm}^{-1}$  in the spectral density of Fig. 1.

High-frequency librational modes of liquid water differentiate it from other polar solvents. The origin of these intermolecular motions of water has been studied extensively. In aqueous solutions, solvation acts on a similar time scale to

the intramolecular modes of the chromophore. Hence, a more complex strategy than we have previously used<sup>35-38</sup> is essential in order to separate these two contributions. In addition, high time resolution is a clear necessity. We have previously shown that photon echo peak shift spectroscopy can resolve sub-pulse duration dynamics,<sup>39</sup> therefore, we employ this technique to study the dynamics of aqueous solvation.

## II. PEAK SHIFT SPECTROSCOPY

The photon echo peak shift measurement is briefly described in this section. A detailed description of this spectroscopy can be found in other studies.<sup>39-43</sup> The peak shift measurement, obtained from the photon echo signal, is generated by a three-pulse interaction with the chromophore. The first pulse,  $\mathbf{k}_1$ , creates a coherence between the ground and excited state. The second pulse,  $\mathbf{k}_2$ , ends the coherence period,  $\tau$ , and initiates a population period (ground or excited state)  $T$  where spectral diffusion can occur. The third pulse,  $\mathbf{k}_3$ , ends the population period and creates another coherence period. The echo signal,  $\mathbf{k}_s$ , is collected in two symmetry-related phase-matching directions,  $\mathbf{k}_1 - \mathbf{k}_2 + \mathbf{k}_3$  and  $-\mathbf{k}_1 + \mathbf{k}_2 + \mathbf{k}_3$ , which correspond to specific spatial locations due to momentum conservation. The peak shift for a particular  $T$  is obtained by determining half the difference between the maximum of the peak positions obtained by scanning  $\tau$ . A nonzero peak shift indicates rephasing ability, i.e., retention of optical transition frequency information.

For a room temperature liquid, in which there are no site energy differences that persist for longer than the experimental time window, the transition frequency of an individual chromophore,  $\omega_{eg}^i(t)$ , is defined as

$$\omega_{eg}^i(t) = \langle \omega_{eg} \rangle + \delta \omega_{eg}^i(t), \quad (1)$$

where  $\langle \omega_{eg} \rangle$  is the average transition frequency and  $\delta \omega_{eg}^i(t)$  is a time dependent fluctuating term. The transition frequency correlation function  $M(t)$  describes the average dynamical fluctuating contribution to the echo signal and is given by

$$M(t) = \frac{\langle \delta \omega_{eg}(0) \delta \omega_{eg}(t) \rangle}{\langle \delta \omega_{eg}^2 \rangle}, \quad (2)$$

where  $\langle \delta \omega_{eg}^2 \rangle$  is the mean square fluctuating amplitude or coupling strength. The fluctuation-dissipation theorem relates  $\delta \omega_{eg}(t)$  to the reorganization energy  $\lambda$ .

Calculating echo signals is commonly performed by either modeling  $M(t)$  as a sum of Gaussian components, exponential decays, and damped cosines,<sup>39</sup> or adopting the Brownian oscillator model.<sup>42</sup> This method is especially appropriate at long times where the peak shift corresponds directly to  $M(t)$ .<sup>40</sup> In most solute-solvent systems, the clear separation of time scales allows a direct correlation of time scales in the peak shift data to dynamical processes. The calculations are further aided by simplification of the cumulant expansion equations using the high temperature limit.<sup>43</sup> However, in this aqueous system, the overlapping time scales and the possible limitations of the classical (high temperature) limit necessitate a more general approach to inter-

pret the data. Therefore, the spectral density  $\rho(\omega)$  is directly used to calculate the response, without assuming a model for  $M(t)$ . The spectral density characterizes the range and distribution of time scales (or frequencies) of solute-solvent interactions which couple to the peak shift observable,  $\langle\omega_{eg}\rangle$ . The relative weight of the spectral density for a given component,  $\rho_i(\omega)$ , is adjusted by scaling the reorganization energy,  $\lambda_i$ , and coupling strength,  $\langle\Delta_i^2\rangle$  according to

$$\lambda_i = \int_0^\infty d\omega \omega \rho_i(\omega) \quad (3)$$

and

$$\langle\Delta_i^2\rangle = \int_0^\infty d\omega \omega^2 \coth\left(\frac{\hbar\beta\omega}{2}\right) \rho_i(\omega), \quad (4)$$

where  $\beta = 1/k_B T$  and  $i$  represents an arbitrary component. Using this approach, a total spectral density  $\rho_{\text{tot}}(\omega)$  is determined. In general, a variety of models can be applied to regard the spectral density obtained from experiment, simulation, or theory.<sup>35</sup>

The dynamical behavior of the system is contained within the line broadening function  $g(t)$ , which can be readily calculated according to

$$g_i(t) = \frac{-i\lambda t}{\hbar} + i \int_0^\infty d\omega \rho_i(\omega) \sin(\omega t) + \int_0^\infty d\omega \rho_i(\omega) \coth\left(\frac{\hbar\beta\omega}{2}\right) [1 - \cos(\omega t)]. \quad (5)$$

The imaginary and real components describe spectral diffusion and spectral broadening, respectively. Dynamical processes are combined to obtain a total  $g(t)$ , which is then inserted into the response functions  $R_1 - R_8$  selected by the echo experiment. The third order polarization is then calculated by convolution of the response functions with the optical fields of the experimental pulse sequence.<sup>39,42</sup> A pulse envelope of 25 fs, the transform limit obtained from the excitation spectral bandwidth, was used in calculating the echo signal. Finally, the peak shift is extracted from the calculated three-pulse photon echo signal and compared with the experiment.

The maximum of the fluorescence spectrum,  $\sigma_f(\omega)$ , is red shifted with respect to the maximum of the absorption spectrum,  $\sigma_a(\omega)$ , by  $2\lambda$  or the Stokes shift.<sup>43</sup> This widely used technique for determining the reorganization energy can provide an accurate value of  $\lambda$  when  $\sigma_a(\omega)$  and  $\sigma_f(\omega)$  are Gaussian, but is ambiguous for asymmetric or structured spectra. Using this method, the observed Stokes shift between the absorption and fluorescence spectra for eosin in water is  $720 \text{ cm}^{-1}$ . However, the absorption spectrum of eosin in water is far from Gaussian (Fig. 5) and half the Stokes shift ( $360 \text{ cm}^{-1}$ ) underestimates the solvent reorganization energy. Therefore, we used a novel method<sup>44</sup> to calculate the reorganization energy according to

$$\lambda_{\text{tot}} = \frac{\int_0^\infty \omega [\sigma_a(\omega) - \sigma_f(\omega)] d\omega}{\int_0^\infty [\sigma_a(\omega) + \sigma_f(\omega)] d\omega}, \quad (6)$$

where the lower integration limit, 0, is defined as the zero-zero energy or the intersection of  $\sigma_a$  and  $\sigma_f$ . A derivation of Eq. (6), the normalized difference of the first moment between the absorption and fluorescence spectra, is presented elsewhere.<sup>44</sup> This procedure explicitly relates the imaginary part of the line broadening function, i.e., the spectral diffusion, to the reorganization energy of the experimental absorption and fluorescence spectra.

### III. EXPERIMENT

The peak shift and transient grating measurements were performed at 3.8 kHz using a regeneratively amplified Ti:sapphire laser<sup>45</sup> to pump an optical parametric amplifier (OPA) arranged in a double pass configuration.<sup>46</sup> The regenerative amplifier produces 800 nm, 50 fs, 25  $\mu\text{J}$ , Gaussian pulses used to pump the OPA optimized at 520 nm (near the absorption maximum of the chromophore). In the amplifier,  $\sim 10\%$  of the pump is focused onto a 2 mm sapphire window to generate continuum. Infrared light, centered at  $\sim 1480 \text{ nm}$ , is combined collinearly with the pump and amplified parametrically in a 4 mm long BBO crystal cut to  $20^\circ$ . After a second pass, the amplified infrared and residual pump are mixed to produce 520 nm via sum frequency generation in a 250  $\mu\text{m}$  BBO cut to  $23^\circ$ . This process is performed collinearly by focusing the beams with an off-axis parabolic mirror ( $f = 3 \text{ in.}$ ). The  $\sim 15 \text{ nm}$  bandwidth pulses were compressed with a pair of F-2 prisms to a pulse duration as short as 30 fs, measured in a 300  $\mu\text{m}$  BBO, Type I, corresponding to a time bandwidth product of 0.54.

The 520 nm beam was split into three beams,  $\mathbf{k}_1$ ,  $\mathbf{k}_2$ , and  $\mathbf{k}_3$  of equal intensity. Period  $\tau$  was scanned from  $-150 \text{ fs}$  to  $150 \text{ fs}$  for a fixed population period  $T$  ranging from 0 to 100 ps. A 25 cm achromatic doublet was used to focus the beams to a spot size of  $\sim 250 \mu\text{m}$ . The total energy of the three beams was  $\sim 15 \text{ nJ}$  at the sample. Both echo directions  $\mathbf{k}_1 - \mathbf{k}_2 + \mathbf{k}_3$  and  $-\mathbf{k}_1 + \mathbf{k}_2 + \mathbf{k}_3$  were simultaneously detected with Si photodiodes, amplified ten times and sampled with gated integrators. A phase-locked chopper modulated beam  $\mathbf{k}_3$ , at 1.9 kHz, and the integrated echo signals were detected with lock-in amplifiers.

The chromophore used in this system is eosin Y. As shown in Fig. 2, eosin, a derivative of fluorescein, contains a xanthene ring system with four bromine substituents. Samples were prepared by dissolving eosin Y in doubly distilled water to an optical density of  $\sim 0.7$ . For a 100  $\mu\text{m}$  cell, this corresponds to a concentration of  $1.44 \times 10^{-4} \text{ M}$  and  $\epsilon(517 \text{ nm}) = 9.7 \times 10^4 \text{ M}^{-1} \text{ cm}^{-1}$ .<sup>47</sup> The sample was rotated in a static 100  $\mu\text{m}$  cell. Measurements were made at room temperature.

### IV. RESULTS

Transient grating measurements, which provide population and solvation dynamics information, were also performed in this study. Figure 2 shows a transient grating measurement of eosin in water as a function of population period. A typical three-pulse photon echo peak shift measurement of eosin in water is shown in Fig. 3. The integrated echo signals are fit to Gaussians, and the peak shift is ex-

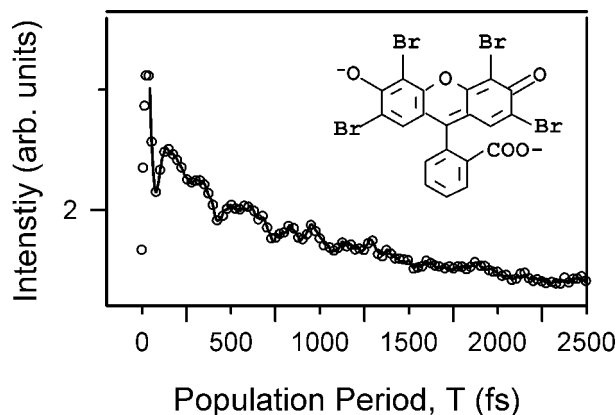


FIG. 2. The transient grating signal of eosin in water (circles) with a linear prediction singular value decomposition fit (solid line) to the data. The structure of the eosin molecule is also shown.

tracted. The initial peak shift position is  $\sim 12$  fs. The peak shift data exhibit a very fast, large amplitude decay to a peak shift of  $\sim 3$  fs where the rate of decay abruptly slows. As shown in the inset of Fig. 3, the peak shift data decay to zero by  $\sim 15$  ps. Oscillations, resulting from the intramolecular vibrational modes of eosin, are also present in the signal. Many measurements were performed in order to confirm reproducibility of the signal. Saturation effects were not observed in the peak shift data. Data sets were shifted ( $\pm 1$  fs) in peak shift in order to compensate for a drift in the peak shift at long population times. The data were also shifted in population period to overlap the oscillations. In some cases, the required shift in the population period was  $\sim 5$  fs and compensates for a small chirp in the 30–35 fs excitation pulse.<sup>48</sup>

## V. SOLVATION

As noted earlier, the overlapping time scales of solvation and vibrational motion make unambiguous extraction of the

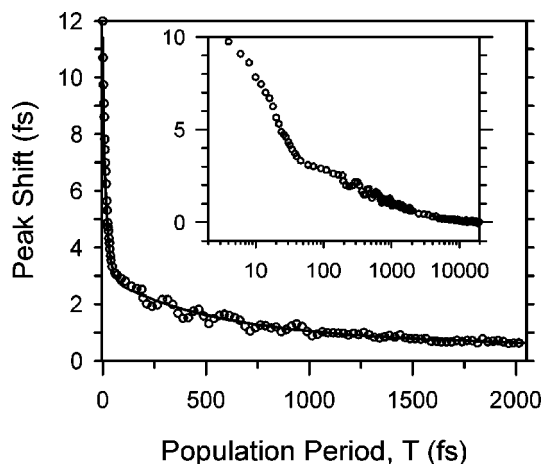


FIG. 3. Three-pulse photon echo peak shift data of eosin in water (circles) are shown with a simple exponential fit (solid line) as a guide to the eye. The fit includes a  $\sim 17$  fs (73%) fast component and two slower components,  $\sim 400$  fs (15%) and  $\sim 2.7$  ps (12%). Note the abrupt change in the slope when the peak shift has decreased to  $\sim 3$  fs. The inset, on a log scale and without fit, shows that the peak shift decays to 0 fs by  $T \sim 15$  ps.

solvation dynamics challenging. Instead of attempting to extract the time scales directly from the peak shift measurement, our approach was to determine if the data were consistent with theoretical predictions for aqueous solvation. Thus, we used a theoretical solvation spectral density, as detailed below, in combination with intramolecular vibrational contributions, as described in Sec. VI, to simulate the data.

The theoretical solvation spectral density, shown in Fig. 1, was calculated using a new perspective of dynamical dielectric continuum theory.<sup>19</sup> To model aqueous solvation dynamics for eosin, an initial guess of the geometry of the chromophore<sup>49</sup> was optimized (using MOPAC) to obtain ground and excited state charge distributions and a change in dipole moment of  $\sim 8$  Debye. Using this optimized geometry, a van der Waals surface ( $\sim 400 \text{ \AA}^3$ ) was adapted to generate a molecular surface for eosin.<sup>50</sup> The frequency dependent response of pure water is obtained from experimental IR data.<sup>11,12,14,51</sup> These ingredients were used to calculate the total solvation energy,  $E(\omega)$ ,<sup>19,52</sup> of eosin in water. A relationship between the solvation energy and the solvation correlation function,  $S(t)$ <sup>53</sup> can be derived<sup>54</sup> and expressed by

$$S(t) = \frac{\hbar}{\lambda} \int_0^\infty d\omega \frac{E''(\omega)}{\omega} \cos(\omega t), \quad (7)$$

where  $E''(\omega)$  is the imaginary portion of the total solvation energy. By expressing  $S(t)$  in terms of a solvation spectral density via

$$S(t) = \frac{\hbar}{\lambda} \int_0^\infty d\omega \omega \rho_{\text{sol}}(\omega) \cos(\omega t) \quad (8)$$

and equating Eq. (7) to Eq. (8), the useful relationship  $\rho_{\text{sol}}(\omega) = E''(\omega)/\omega^2$  is readily obtained. Recall, in the classical limit,  $S(t)$  and  $M(t)$ , Eq. (2), are equivalent. Correspondingly, the solvation spectral density in Fig. 1 is calculated directly from the aqueous solvation energy.

The solvation spectral density is inserted into the line broadening function, Eq. (5), and a peak shift is calculated as outlined in Sec. II. The calculated peak shift arising from the solvation contribution alone is compared to the experimental data in Fig. 4. This confirms that the fast and intermediate (50–500 fs) time scales in the data can be reproduced *solely* with the solvation spectral density. Interestingly, an abrupt change in the rate of decay of the experimental data at a peak shift of  $\sim 3$  fs is predicted by the theoretical solvation spectral density. During the population period from 80 to 180 fs, the system shows no evidence of dephasing, which will be further addressed in Sec. VII. However, as shown in the inset of Fig. 4, the simulated peak shift decays to nearly zero by  $\sim 2$  ps, whereas the experimental data exhibits a nonzero peak shift until  $\sim 15$  ps. The calculated absorption spectrum (solid line) is compared with the experimental absorption spectrum (circles) in Fig. 5. Solvation alone captures the general shape of the eosin absorption spectrum, but clearly does not reproduce the vibrational shoulder on the high-frequency side.

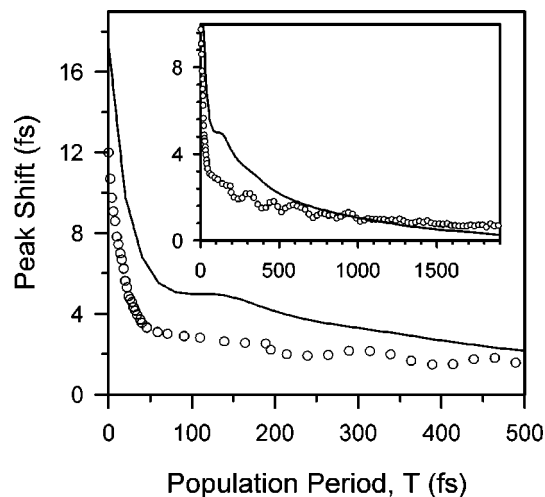


FIG. 4. Comparison of the simulated peak shift (solid line) using the theoretical solvation spectral density alone to the experimental data (circles). Note the correspondence of the initial time scales. The delayed rate of decay of the peak shift at  $\sim 3$  fs is predicted by theory and arises from the  $180\text{ cm}^{-1}$  hindered translational band of water. The tail evident in the peak shift data is not reproduced by this solvation spectral density alone (inset).

## VI. SOLVATION AND INTRAMOLECULAR PROCESSES

While solvation captures many of the general features of the data, it is clear that additional nuclear degrees of freedom contribute to the observed peak shift. Intramolecular vibrations of eosin, as evident from the oscillations in the peak shift data and from the shoulder in the absorption spectrum, contribute to the dynamics of the system. This shoulder is partly attributed to ring breathing modes of eosin centered around  $1500\text{ cm}^{-1}$ .<sup>55</sup> The data further exhibit a long decay component, which was not captured by the theoretical solvation spectral density. This diffusive tail is treated as an additional solvation component, i.e., an intermolecular contribution.

In order to completely describe the dynamics of the chromophore-solvent system, two spectral densities are com-

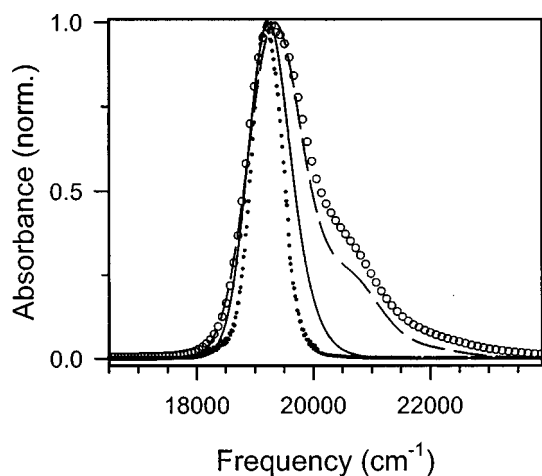


FIG. 5. A comparison of the experimental (circles) to the calculated (lines) absorption spectra. The calculated spectra are from solvation alone (solid line) and a simulation including solvation and intramolecular vibrations (dashed line) using parameters of Fig. 6(b). The laser excitation spectrum is also shown (solid circles).

bined: one for water solvation  $\rho_{\text{solv}}(\omega)$  and the second for the intramolecular vibrations of eosin  $\rho_{\text{vib}}(\omega)$  into a total spectral density,  $\rho_{\text{tot}}(\omega) = \alpha_{\text{solv}}\rho_{\text{solv}}(\omega) + \alpha_{\text{vib}}\rho_{\text{vib}}(\omega)$ . Specific characteristics in the peak shift data and absorption spectrum constrain the coefficients, thereby constraining the coupling strength and reorganization energy [according to Eqs. (3) and (4), respectively] of both dynamical processes. More specifically, the amplitude of the oscillations in the peak shift constrain the coupling strength for impulsively excited vibrations, and the fast components of the peak shift confine the coupling of the solvation spectral density. The width of the absorption spectrum is a further limitation on both processes and is constrained by the total reorganization energy, determined using Eq. (6), of  $877\text{ cm}^{-1}$ . We scaled the solvation spectral density  $\rho_{\text{solv}}(\omega)$ , by a total rms value of the coupling strength ( $\Delta_{\text{solv}} = 436\text{ cm}^{-1}$ ) and a total reorganization energy of  $\lambda_{\text{solv}} = 360\text{ cm}^{-1}$ . When a value above  $500\text{ cm}^{-1}$  is used for  $\Delta_{\text{solv}}$ , the peak of the simulated absorption spectrum is too wide.

The solvation spectral density was included from Fig. 1 with a modification to include the slow component evident in the tail of the peak shift. Although the initial dynamics is Gaussian,<sup>39,40,42</sup> an exponential fit to the peak shift data was performed to characterize this slow component. The fit included a  $\sim 17$  fs (73%) fast component and two slower components,  $\sim 400$  fs (15%) and  $\sim 2.7$  ps (12%). This simple fit, as shown in Fig. 3, provides time constants and amplitudes for times larger than the bath correlation time and can be related to our solvation contribution. By comparing the exponential fit to the experimental peak shift data with a fit to the simulated peak shift, calculated using  $\rho_{\text{solv}}(\omega)$ , an additional 8 ps component is necessary to equate the two fits. The spectral density for this component, Fig. 6(b), was constructed by assuming the functional form of an overdamped Brownian oscillator with an amplitude  $\lambda_i = 130\text{ cm}^{-1}$  and an inverse correlation time of  $(\Lambda_i)^{-1} = 8\text{ ps}$ .<sup>56</sup> This additional contribution was added to the original solvation spectral density to form a new total solvation spectral density.

The vibrational spectral density  $\rho_{\text{vib}}(\omega)$  was constructed by combining information present in the oscillations of the peak shift as well as frequencies obtained from the transient grating and Raman measurements of eosin. Determining the vibrational contribution to the spectral density is complicated by the fact that the laser pulse (Fig. 5) impulsively excites only a portion of the total vibrational spectrum. The total vibrational contribution was separated into two parts. Impulsively excited vibrations, those which have a period of oscillation longer than the pulse duration, are ultimately determined from a direct fit of damped cosine functions to the peak shift. The non-impulsively excited intramolecular vibrations, however, are obtained from the Raman spectrum.

To determine the impulsively excited vibrations (frequencies, amplitudes, phases and damping times), the transient grating response (Fig. 2) is analyzed using linear prediction singular value decomposition. The identified frequencies and amplitudes are compared with the vibrational modes of the Raman and infrared spectra of eosin. These modes and damping times are then used as initial pa-

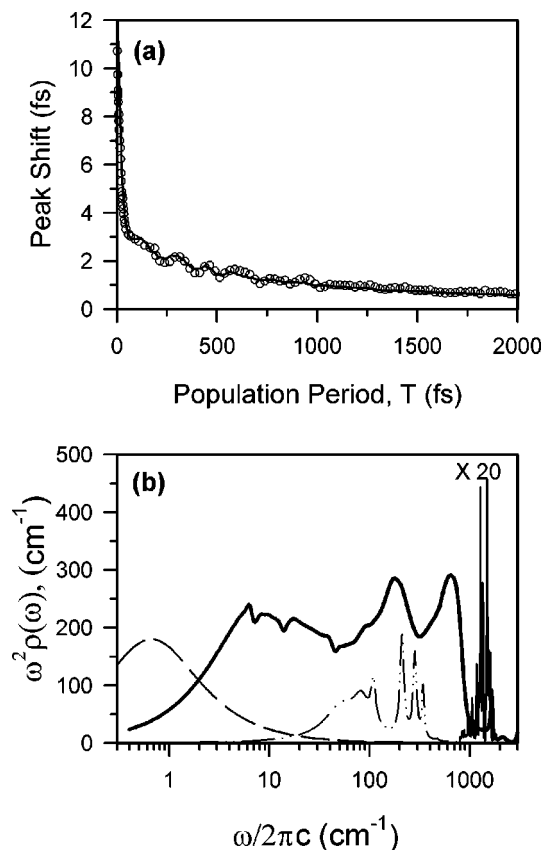


FIG. 6. (a) Comparison of the simulated peak shift (solid line) to the experimental data (circles). (b) The coupling strength weighted spectral density  $\rho(\omega)\omega^2$  includes a theoretical solvation contribution with  $\lambda = 360 \text{ cm}^{-1}$  (dark solid line), an 8 ps diffusive intermolecular component with  $\lambda = 130 \text{ cm}^{-1}$  (dashed line), the impulsively excited vibrations with  $\lambda = 58 \text{ cm}^{-1}$  (dashed-dotted line), and high-frequency intramolecular vibrations with  $\lambda = 300 \text{ cm}^{-1}$  (light solid line).

rameters for a direct fit of damped cosine functions to the peak shift data. A vibrational spectral density was constructed from 0 to  $500 \text{ cm}^{-1}$  with these parameters.<sup>57</sup> Very low amplitude intermediate modes ( $500\text{--}800 \text{ cm}^{-1}$ ) were resolved in the analysis of the transient grating data, but not resolved in the peak shift measurements. When these modes were artificially included with small coupling strength, structure not visible in the peak shift data arose. Since this echo measurement did not impulsively excite frequencies above  $500 \text{ cm}^{-1}$ , this range was excluded in this spectral density. The coupling strength and phases of the impulsively excited vibrations were adjusted to overlap the oscillations in the data. The parameters used in constructing this vibrational spectral density  $\rho_{\text{vib}}(\omega)$  are provided in Table I. The photon echo experiment inherently contains phase information, but  $\rho(\omega)$  should not carry any phase information.<sup>38</sup> As a result, the phases in Table I were set to zero before transforming the oscillations to a spectral density. The spectral density for the intramolecular vibrations is shown in Fig. 6(b).

The spectral density of non-impulsively excited vibrations is taken directly from the Raman spectrum of eosin [Fig. 6(b)]. High-frequency intramolecular vibrations ( $800\text{--}2000 \text{ cm}^{-1}$ ), including ring-breathing modes, destructively interfere within the first tens of femtoseconds and contribute

TABLE I. Input parameters used to create the impulsively excited contribution to the vibrational spectral density  $\rho_{\text{vib}}(\omega)$  for three-pulse photon echo simulations. Frequency ( $\omega$ ), rms coupling strength ( $\Delta$ ), phase ( $\Phi$ ) and damping times ( $\Gamma$ ) were obtained from a fit of damped cosine functions to the peak shift. The values in this table were inserted into the equation in Ref. 57 to generate the spectral density by a procedure outlined in the text.

$\omega \text{ (cm}^{-1}\text{)}$	$\Delta \text{ (cm}^{-1}\text{)}$	$\Phi \text{ (radians)}$	$\Gamma \text{ (fs)}$
46	114	-0.69	221
80	78	-0.80	279
109	49	-0.30	730
210	70	-0.29	469
283	61	0.223	404
342	40	0.035	498
474	7	0.51	442

to the amplitude of the ultrafast component in the data. The large coupling strength for this range is essential in order to capture the appearance of a vibrational shoulder on the high-frequency side of the absorption spectrum and slightly improves our ability to simulate the initial peak shift data. Since our pulse spectrum does not span the entire absorption spectrum, these vibrations are only partially excited by the optical field of our experimental pulses.

Simulations were performed to determine the coupling strength  $\langle \Delta^2 \rangle$  and reorganization energy of each contribution that best reproduces the peak shift data and absorption spectrum. Figure 6(b) provides the spectral density contributions used to simulate the peak shift data. The calculated and experimental peak shift data for eosin in water are shown in Fig. 6(a). The simulated peak shift includes the theoretical solvation spectral density, the 8 ps component, and the intramolecular vibrations. As Fig. 6(a) shows, the abrupt decrease in the rate of decay between  $T = 40\text{--}80 \text{ fs}$ , or at a peak shift of  $\sim 3 \text{ fs}$ , is captured by the simulated peak shift, giving confidence that the dynamical origin of this feature is well determined. The minor deficiency in the amplitude of the oscillations of the peak shift simulation originates in the contribution of the intramolecular modes of eosin which have not been entirely characterized. The large dynamical range of the simulation, verified by the excellent fit up to 10 ps (not shown), allows an accurate description of the diffusive tail. The reorganization energy used in the simulation,  $\lambda = 848 \text{ cm}^{-1}$ , produces a reliable description of the absorption spectrum, as shown in Fig. 5, and is within the upper limit provided by the total reorganization energy of  $877 \text{ cm}^{-1}$ . The calculated absorption spectrum reproduces the width of the peak and a portion of the shoulder. Models that reconstruct the entire absorption spectrum, i.e., simulate the entire shoulder, do not reproduce the peak shift data. This implies that not all the high-frequency vibrations on the blue edge of the spectrum were excited. Therefore, they are not evident in the peak shift data, and a value smaller than the total reorganization energy was used. Finally, the same line broadening function simulates the experimental fluorescence spectrum, which, for the eosin-water system, is merely the mirror image of the absorption spectrum.

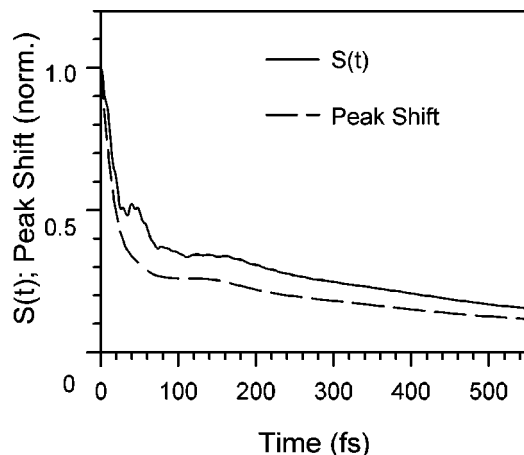


FIG. 7. The comparison of the normalized simulated peak shift (dashed line) to the theoretically determined solvation relaxation function  $S(t)$  (solid line) calculated according to Eq. (8). Note the difference in the decay rates at short times and the recurrence at  $\sim 40$  fs in  $S(t)$  due to the librational band in water.

## VII. DISCUSSION AND CONCLUSIONS

The experimental peak shift measurement shows that the majority of the aqueous solvation response occurs on an ultrafast time scale. The correspondence between the theoretical solvation spectral density, constructed from a formulation of dielectric continuum theory,<sup>19</sup> and the data is remarkable. These experimental data, as will be discussed below, confirm our dielectric continuum results, which predict a very rapid (within  $\sim 30$  fs) decay contributing to  $\sim 60\%$  of the total solvent relaxation. The peak shift data also illustrate that aqueous solvation dynamics is complete by  $\sim 15$  ps.

It is important to re-emphasize that the initial time dependence of the peak shift does not correspond to the solvation times [as do  $S(t)$  or  $M(t)$ ].<sup>39</sup> When compared to  $S(t)$  in the classical limit, the three-pulse photon echo decay overestimates the amplitude and underestimates the time scale of the initial peak shift.<sup>39</sup> Moreover, a third order experiment is rather insensitive to the detailed form of the time dependence, i.e., the echo measurements cannot differentiate a Gaussian from an exponential at short times.<sup>35,38</sup> Therefore, a quantitative interpretation of the ultrafast aqueous solvation component can only be obtained by a rigorous analysis of the solvation relaxation function. The calculations used a theoretical solvation spectral density to calculate a peak shift. However, as illustrated in Eq. (8), this same solvation spectral density can also be used to obtain  $S(t)$ . For the purpose of illustrating the difference between  $S(t)$  and the peak shift, the long time portion of the peak shift was normalized to  $S(t)$  and is shown in Fig. 7. The theoretically determined  $S(t)$  was fit to one Gaussian and two exponentials; the ultrafast portion of this result—a 28 fs component with 58% of the decay amplitude provides a more accurate quantitative measure of the solvation when compared to the ultrafast component of the peak shift fit—a 17 fs (73%).

Another interesting feature in Fig. 7 is the peak between 40 and 70 fs in  $S(t)$  that corresponds to the broad librational band of water centered about  $600\text{ cm}^{-1}$ . The mathematical convolution with the finite, 25 fs, pulse duration of the ex-

periment averages out this band in the simulated peak shift. However, this peak is resolved in a simulated peak shift when a nearly impulsive limit ( $\sim 10$  fs pulse duration) is applied. This recurrence, observed only in the simulation, occurs at  $\sim 40$  fs and resembles a similar feature, also at  $\sim 40$  fs, in the pump-probe data of the hydrated electron.<sup>58–61</sup> This implies that the hydrated electron and a polar solute have a similar ultrafast aqueous solvation response as previously suggested.<sup>41</sup>

The striking agreement between the photon echo peak shift data and the dielectric continuum theory at early population times ( $T=40\text{--}180$  fs), or at a peak shift value of  $\sim 3$  fs, will now be discussed. Both theory and experiment show a drastic change in the slope of the peak shift between  $T=40$  and 80 fs. When the  $180\text{ cm}^{-1}$  band of the aqueous solvation spectral density is excluded from the simulation, the calculated peak shift becomes an evenly decaying function and fails to capture the abrupt change in the rate of decay at a peak shift of 3 fs. While a fit to damped cosines for both the peak shift and the transient grating data required a frequency of approximately  $180\text{ cm}^{-1}$ , the Raman and IR spectra of eosin validate the absence of a  $180\text{ cm}^{-1}$  vibrational mode arising from the probe molecule. Therefore, this prominent feature in both experimental data and theoretical predictions is not an intramolecular vibrational mode of the probe molecule. Instead, it corresponds to the low-frequency hindered translational band ( $\sim 180\text{ cm}^{-1}$ ) resulting from dipole-induced-dipole interactions in water. The signature of the  $\sim 180\text{ cm}^{-1}$  underdamped solvent mode was not resolved in the experiments of the hydrated electron.<sup>58–61</sup>

Calculations of Raman intensity using a polarizability expansion performed by both Madden *et al.*<sup>20</sup> and Mazzacurati *et al.*<sup>21</sup> each ascribe the majority of the amplitude of this hindered translational band to dipole-induced-dipole effects. Mukamel extends this discussion by showing that anisotropic polarizability provides a more accurate Raman amplitude of this hindered translational peak.<sup>23</sup> Our experimental data corroborate the studies of Bagchi and co-workers,<sup>24,25</sup> which predicted that the interaction-induced polarizability effects in water slow the initial decay of the dynamics in the same  $\sim 180\text{ cm}^{-1}$  region and play a significant role in determining the initial inertial aqueous response. Our data show similar structure to recent simulations,<sup>26</sup> which include the effects of polarizability fluctuations on the nuclear Kerr response of water, and show short-time structure in the optical response. Moreover, peak shift measurements of water substantiate the strong influence of the dipole-induced-dipole contribution as theoretically predicted.

As previously discussed, the peak shift data deviate slightly from the theoretical prediction in the long time dynamics. The 8 ps exponential component, added to simulate the tail of the peak shift data, may arise from water tightly associated with the eosin molecule. Eosin is both doubly charged and quite polarizable.<sup>62</sup> Hence, a strong interaction with the hydrogen bonding solvent is almost inevitable.<sup>63</sup> It has been suggested that the slow reorientation of eosin, com-

pared to other cations of the same size, arises from the attachment of water molecules to the eosin.<sup>63</sup> Accordingly, it is possible that the molecular volume of the dye is considerably larger than that estimated by the van der Waals surface used in the dielectric continuum theory. Solvation models that include polarizability of the solute show a modest increase in the solvation time scale.<sup>34,64</sup> Combining the results of Refs. 34 and 63 with typical polarizability values,<sup>65</sup> we predict a minor effect on the dynamics of eosin in water. More detailed models of this system should include the increased molecular volume and the solute polarizability. Such calculations could yield a more precise origin of the 8 ps component, but are beyond the present scope of this work.

Vibrational cooling of the probe molecule, occurring on the picosecond time scale, is another possible explanation for this additional 8 ps component. Experimental results, using pump-probe, fluorescence up-conversion, resonance Raman, and hole burning have demonstrated that intramolecular redistribution of energy leads to a population of the vibrational manifold that is characterized by a temperature higher than the surrounding solvent.<sup>66</sup> Moreover, these vibrationally "hot" molecules have been shown to cool on the picosecond time scale by collisional interactions with solvent molecules.<sup>66</sup> To the best of our knowledge, past solvation studies have not clearly demonstrated this effect, but studies of dye molecules have shown that excess energies of 1000–3500 cm<sup>-1</sup> per molecule correspond to vibrational cooling times of 1–10 ps.<sup>67</sup> Because the aqueous solvation decay follows nearly identical dynamics when an excess of ~800 cm<sup>-1</sup> of energy is applied, i.e., the excitation wavelength is tuned from 520 nm to 535 nm, this explanation seems less viable.

Although a molecular level description of aqueous solvation is far from complete, the dominance of the ultrafast component has significant implications for reaction dynamics in a variety of chemical systems. Since water is the natural solvent of biological processes, the importance of understanding aqueous solvation cannot be overemphasized. Further experimental work to characterize solvation dynamics in complex biological systems is underway.<sup>68</sup>

## ACKNOWLEDGMENTS

Experimental aspects of this collaborative research were supported, in part, by the National Science Foundation. Theoretical aspects carried out by X.S. were supported by the U.S. Department of Energy, Office of Basic Energy Science. M.J.L. acknowledges support from a GAANN Fellowship and thanks Dr. Jae-Young Yu for many helpful discussions.

<sup>1</sup>P. F. Barbara and W. Jarzaba, *Adv. Photochem.* **15**, 1 (1990).

<sup>2</sup>R. Jimenez, G. R. Fleming, P. V. Kumar, and M. Maroncelli, *Nature (London)* **369**, 471 (1994).

<sup>3</sup>B. Zolotov, A. Gan, B. D. Fainberg, and F. D. Huppert, *Chem. Phys. Lett.* **265**, 418 (1997).

<sup>4</sup>Y. J. Chang and E. W. Castner, Jr., *J. Chem. Phys.* **99**, 113 (1993).

<sup>5</sup>S. Palese, L. Schilling, R. J. D. Miller, P. R. Staver, and W. T. Lotshaw, *J. Phys. Chem.* **98**, 6308 (1994).

<sup>6</sup>L. Thrane, R. H. Jacobsen, P. U. Jepsen, and S. R. Keiding, *Chem. Phys. Lett.* **240**, 330 (1995).

<sup>7</sup>J. T. Kindt and C. A. Schmuttenmaer, *J. Phys. Chem.* **100**, 10373 (1996).

<sup>8</sup>D. M. Carey and G. M. Korenowski, *J. Chem. Phys.* **108**, 2669 (1998).

<sup>9</sup>K. Mizoguchi, Y. Hori, and Y. Tominaga, *J. Chem. Phys.* **97**, 1961 (1992).

<sup>10</sup>G. E. Walrafen, *J. Phys. Chem.* **94**, 2237 (1990).

<sup>11</sup>G. M. Hale and R. M. Querry, *Appl. Opt.* **12**, 555 (1973).

<sup>12</sup>M. N. Afsar and J. B. Hasted, *Infrared Phys.* **18**, 835 (1978).

<sup>13</sup>J. B. Hasted, S. K. Husain, F. A. M. Frescura, and J. R. Birch, *Chem. Phys. Lett.* **118**, 622 (1985).

<sup>14</sup>J. B. Hasted, S. K. Husain, F. A. M. Frescura, and J. R. Birch, *Infrared Phys.* **27**, 11 (1987).

<sup>15</sup>J. E. Bertie and Z. D. Lan, *Appl. Spectrosc.* **50**, 1047 (1996).

<sup>16</sup>I. Ohmine and H. Tanaka, *Chem. Rev.* **93**, 2545 (1993).

<sup>17</sup>M. Maroncelli and G. R. Fleming, *J. Chem. Phys.* **89**, 5044 (1988).

<sup>18</sup>J. S. Bader and D. Chandler, *Chem. Phys. Lett.* **157**, 501 (1989).

<sup>19</sup>X. Song and D. Chandler, *J. Chem. Phys.* **108**, 2594 (1998).

<sup>20</sup>P. A. Madden and R. W. Impey, *Chem. Phys. Lett.* **123**, 502 (1986).

<sup>21</sup>V. Mazzacurati, M. A. Ricci, G. Ruocco, and M. Sampoli, *Chem. Phys. Lett.* **159**, 383 (1989).

<sup>22</sup>B. Guillot, *J. Chem. Phys.* **95**, 1543 (1991).

<sup>23</sup>W. B. Bosma, L. E. Fried, and S. Mukamel, *J. Chem. Phys.* **98**, 4413 (1993).

<sup>24</sup>N. Nandi, S. Roy, and B. Bagchi, *J. Chem. Phys.* **102**, 1390 (1995).

<sup>25</sup>S. Roy and B. Bagchi, *J. Chem. Phys.* **99**, 9938 (1993).

<sup>26</sup>B. D. Bursulaya and H. J. Kim, *J. Phys. Chem. B* **101**, 10994 (1997).

<sup>27</sup>S. Saito and I. Ohmine, *J. Chem. Phys.* **106**, 4889 (1997).

<sup>28</sup>M. Cho, G. R. Fleming, S. Saito, I. Ohmine, and R. M. Stratt, *J. Chem. Phys.* **100**, 6672 (1994).

<sup>29</sup>J. Lobaugh and G. A. Voth, *J. Chem. Phys.* **106**, 2400 (1997).

<sup>30</sup>H. Tanaka and J. Ohmine, *Chem. Phys.* **91**, 6318 (1989).

<sup>31</sup>S. A. Passino, Y. Nagasawa, T. Joo, and G. R. Fleming, *J. Phys. Chem.* **101**, 725 (1996).

<sup>32</sup>S. J. Rosenthal, R. Jimenez, G. R. Fleming, P. V. Kumar, and M. Maroncelli, *J. Mol. Liq.* **60**, 25 (1994).

<sup>33</sup>T. Fonseca and B. M. Ladanyi, *J. Mol. Liq.* **60**, 1 (1994).

<sup>34</sup>P. V. Kumar and M. Maroncelli, *J. Chem. Phys.* **103**, 3038 (1995).

<sup>35</sup>S. A. Passino, Y. Nagasawa, and G. R. Fleming, *J. Chem. Phys.* **107**, 6094 (1997).

<sup>36</sup>Y. Nagasawa, S. A. Passino, T. Joo, and G. R. Fleming, *J. Chem. Phys.* **106**, 4840 (1997).

<sup>37</sup>G. R. Fleming, S. A. Passino, and Y. Nagasawa, *Philos. Trans. R. Soc. London, Ser. A* **356**, 389 (1998).

<sup>38</sup>Y. Nagasawa, J.-Y. Yu, and G. R. Fleming, *J. Chem. Phys.* **109**, 6175 (1998).

<sup>39</sup>T. Joo, Y. Jia, J.-Y. Yu, M. J. Lang, and G. R. Fleming, *J. Chem. Phys.* **104**, 6089 (1996).

<sup>40</sup>M. Cho, J.-Y. Yu, Y. Nagasawa, S. A. Passino, and G. R. Fleming, *J. Phys. Chem.* **100**, 11944 (1996).

<sup>41</sup>G. R. Fleming and M. Cho, *Annu. Rev. Phys. Chem.* **47**, 109 (1996).

<sup>42</sup>W. P. de Boeij, M. S. Pshenichnikov, and D. A. Wiersma, *J. Phys. Chem.* **100**, 11806 (1996).

<sup>43</sup>S. Mukamel, *Principles of Nonlinear Optical Spectroscopy* (Oxford University Press, New York, 1995).

<sup>44</sup>X. Song, *J. Chem. Phys.* (submitted).

<sup>45</sup>T. Joo, Y. Jia, and G. R. Fleming, *Opt. Lett.* **20**, 389 (1995).

<sup>46</sup>V. V. Yakovlev, B. Kohler, and K. R. Wilson, *Opt. Lett.* **19**, 2000 (1994).

<sup>47</sup>A. G. Kepka and L. I. Grossweiner, *Photochem. Photobiol.* **18**, 49 (1973).

<sup>48</sup>C. J. Bardeen, Q. Wang, and C. V. Shank, *J. Phys. Chem. A* **102**, 2759 (1998).

<sup>49</sup>K. Hirano, *Bull. Chem. Soc. Jpn.* **56**, 850 (1983).

<sup>50</sup>M. J. E. Sternberg, *Protein Structure Prediction: A Practical Approach* (IRL Press at Oxford University Press, Oxford, 1996).

<sup>51</sup>The complete set of experimental dielectric data used to calculate the solvation energy is provided in Fig. 1 of X. Song and R. A. Marcus, *J. Chem. Phys.* **99**, 7768 (1993).

<sup>52</sup>X. Song, D. Chandler, and R. A. Marcus, *J. Phys. Chem.* **100**, 11954 (1996).

<sup>53</sup>The solvation correlation function is defined as  $S(t) = [\Delta\bar{E}(t) - \Delta\bar{E}(\infty)] / [\Delta\bar{E}(0) - \Delta\bar{E}(\infty)]$  where  $\Delta\bar{E}(t)$  is the non-equilibrium energy difference between ground and excited states.

<sup>54</sup>Equation (7) can be derived using the expression of Ref. 53 and Eq. (2.7b) of Ref. 52.



- <sup>55</sup>G. R. Fleming, A. W. E. Knight, J. M. Morris, R. J. S. Morrison, and G. W. Robinson, *J. Am. Chem. Soc.* **99**, 4306 (1976).
- <sup>56</sup>The spectral density for the overdamped Brownian oscillator was obtained using Eq. (8.47) of Ref. 43:  $\rho(\omega) = 2\lambda[\omega\Lambda/(\omega^2 + \Lambda^2)]$ .
- <sup>57</sup>The vibrational spectral density, using Eq. (13) of Ref. 36, is calculated for an exponentially damped cosine according to (setting  $\phi$  equal to zero):  $\rho(\omega) = (2/\pi) [\omega^{-2} \tanh(\hbar\beta\omega/2) \langle \Delta^2 \rangle / \pi(\omega_i^2 - \omega^2 + \Gamma_i^2)^2 + 4\omega^2\Gamma_i^2][(\Gamma_i^3 + \omega^2\Gamma_i + \omega_i^2\Gamma_i)\cos\phi_i - (\omega_i^3 - \omega^2\omega_i + \Gamma_i^2\omega_i)\sin\phi]$ .
- <sup>58</sup>C. Silva, P. K. Walhout, K. Yokoyama, and P. F. Barbara, *Phys. Rev. Lett.* **80**, 1086 (1998).
- <sup>59</sup>K. Yokoyama, C. Silva, D. H. Son, P. K. Walhout, and P. F. Barbara, *J. Phys. Chem. A* **102**, 6957 (1998).
- <sup>60</sup>M. F. Emde, A. Baltuska, A. Kummrow, M. S. Pshenichnikov, and D. A. Wiersma, *Phys. Rev. Lett.* **80**, 4645 (1998).
- <sup>61</sup>A. Kummrow, M. F. Emde, A. Baltuska, M. S. Pshenichnikov, and D. A. Wiersma, *J. Phys. Chem. A* **102**, 4172 (1998).
- <sup>62</sup>M. S. Marincesco, *J. Chem. Phys.* **24**, 593 (1927).
- <sup>63</sup>G. R. Fleming, J. M. Morris, and G. W. Robinson, *Chem. Phys.* **17**, 91 (1976).
- <sup>64</sup>B. D. Bursulaya and H. J. Kim, *J. Phys. Chem.* **100**, 16451 (1996).
- <sup>65</sup>W. Liptay, *Excited States* (Academic, New York, 1974).
- <sup>66</sup>T. Elsaesser and W. Kaiser, *Annu. Rev. Phys. Chem.* **42**, 83 (1991).
- <sup>67</sup>F. Laermer, T. Elsaesser, and W. Kaiser, *Chem. Phys. Lett.* **156**, 381 (1989).
- <sup>68</sup>X. J. Jordanides, M. J. Lang, X. Song, and G. R. Fleming (to be submitted).